Vectorized Schemes for Conical Potential Flow Using the Artificial Density Method

Pamela F. Bradley,* Douglas L. Dwoyer,† and Jerry C. South Jr.‡
NASA Langley Research Center, Hampton, Virginia
and
Joseph M. Keen§
Virginia Polytechnic Institute and State University, Blacksburg, Virginia

A method is developed to determine solutions to the full-potential equation for steady supersonic conical flow using the artificial density method. Various update schemes used generally for transonic potential solutions are investigated. The schemes are compared for speed and robustness. All versions of the computer code have been vectorized and are currently running on the CYBER-203 computer. The update schemes are vectorized, where possible, either fully (explicit schemes) or partially (implicit schemes). Since each version of the code differs only by the update scheme and elements other than the update scheme are completely vectorizable, comparisons of computational effort and convergence rate among schemes are a measure of the specific scheme's performance. Results are presented for circular and elliptical cones at angle of attack for subcritical and supercritical crossflows.

Introduction

THE computational solution of steady supersonic conical potential flow has been approached from several different directions using either the conservative or nonconservative approach. The previous conservative methods generally fit the bow shock. Cross-flow shocks are most often captured. Grossman[1] and Siclari[2] have developed codes using the nonconservative formulation of the full potential equation for conical and three-dimensional flows, respectively. Grossman used successive line overrelaxation (SLOR) as the update scheme for the potential, and Siclari investigated the effectiveness of the approximate-factorization (AF) schemes for this problem. Siclari showed both AF1 and AF2 (using the notation introduced in Ref. 2) to be generally faster than SLOR, with AF1 faster than AF2. Sritharan[3] approached the problem using the conservative approach with a Jameson-type artificial viscosity formulation[4] to provide dissipation in supersonic regions. The update scheme was line relaxation with mesh refinement to speed convergence. Shankar[5] also developed a conservative scheme for conical and three-dimensional flows. Although Shankar's code originally used the artificial density formulation of Hafez,[6] his current code introduces artificial viscosity through the density term using a switching scheme based on characteristics theory. Shankar also used approximate factorization for the update scheme.

A method is developed here to obtain solutions for supersonic conical flow using the three-dimensional, steady, compressible, full-potential equation in conservative nondimensional form and the artificial density method. All shocks are captured. Those schemes studied are: successive line overrelaxation (SLOR), checkerboard successive overrelaxation (CKSOR), approximate factorization 1 (AF1), and approximate factorization 2 (AF2). The question is posed here as to whether or not the explicit schemes can become comparable to or better than the implicit schemes in overall computing times if both types of schemes are vectorized (either completely or partially) and processed on vector computers. A slight advantage through vector processing noticeable in this quasi-three-dimensional (conical flow) problem could become a significant advantage for extension to general three-dimensional flows. A stability restriction for the intermediate body boundary condition in the AF2 scheme as investigated by South and Hafez[7] has been applied to the conical flow problem and shown to be valid.

Presented as Paper 84-0162 at the AIAA 22nd Aerospace Sciences Meeting, Reno, NV, Jan. 9-12, 1984; received Feb. 19, 1984; revision received Feb. 19, 1985. This paper is declared a work of the U.S. Government and therefore is in the public domain.

*Aerospace Engineer, Computational Methods Branch, High-Speed Aerodynamics Division. Member AIAA.
†Head, Computational Methods Branch, High-Speed Aerodynamics Division. Associate Fellow AIAA.
‡Chief Scientist. Associate Fellow AIAA.
§NASA Graduate Student Researcher.

Analysis

The governing equation used in this study is the three-dimensional, steady, compressible, potential equation, which in Cartesian coordinates and conservative nondimensional form is

$$\frac{\partial}{\partial x}\left[\rho\left(\frac{\partial\phi}{\partial x}+V_{x_\infty}\right)\right]+\frac{\partial}{\partial y}\left[\rho\left(\frac{\partial\phi}{\partial y}+V_{y_\infty}\right)\right]+\frac{\partial}{\partial z}\left[\rho\left(\frac{\partial\phi}{\partial z}+V_{z_\infty}\right)\right]=0 \tag{1}$$

where ρ is the isentropic density defined subsequently, ϕ the disturbance velocity potential, and V_{x_∞}, V_{y_∞}, V_{z_∞}, the free-stream velocity components. The isentropic density is given by

$$\rho=\left[1-\frac{\gamma-1}{2}M_\infty^2\left(V^2-1\right)\right]^{1/(\gamma-1)} \tag{2}$$

where γ is the ratio of specific heats. For the problem of interest here, Eq. (1) must be transformed into more convenient coordinates, a discrete approximation formed, and a solution procedure developed for the resulting nonlinear algebraic system. Details of these steps are outlined below.

Transformation of Governing Equations

The natural coordinate system for conical flow is spherical coordinates $(\bar{R},\Gamma,\psi)$ (Fig. 1) which are defined in terms of

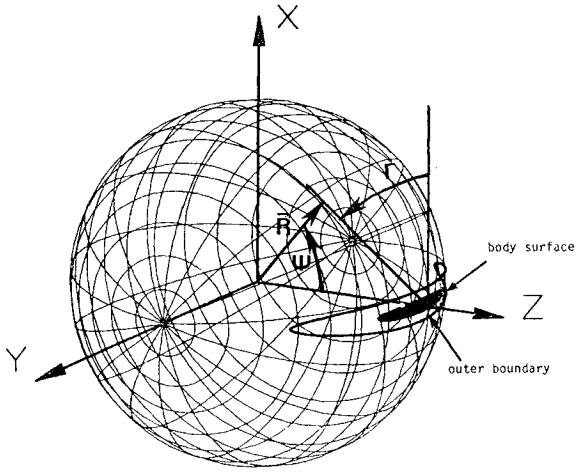

Fig. 1 Spherical coordinates.

the Cartesian coordinates (x,y,z) used in Eq. (1) as:

$$x=\bar{R}\cos\Gamma\sin\psi, \qquad y=\bar{R}\sin\Gamma\sin\psi, \qquad z=\bar{R}\cos\psi \tag{3}$$

The axis of the cone is along the z axis where $\psi=0$ and the body is defined on the surface of a sphere, $\bar{R}=\text{const}$. Although the spherical coordinates naturally fit the conical flow problem, a solution to the exact potential equation with exact boundary conditions for general conical bodies would be more conveniently handled if the body surface were a coordinate line. One way for the body surface to be a coordinate line is by conformal mapping. One conformal mapping, which transforms the spherical coordinates to a surface (p,q), is the stereographic projection of Weatherburn[8] as presented by Grossman[1] (Fig. 2):

$$p+iq=\tan(\psi/2)e^{i\Gamma} \tag{4}$$

This mapping is followed by a second conformal mapping to allow general body cross sections to be coordinate lines. The metric resulting from these transformations, H, is given by,

$$H=\frac{\sin\psi}{\tan\psi/2}\,h(r,\theta) \tag{5}$$

where $h(r,\theta)=1$ for circles and must be derived in some manner for other conical bodies. A simple formulation for $h(r,\theta)$ was suggested by Jameson[4] for general bodies in the σ plane. For example, the transformation from a circle to an ellipse can be determined easily using the Joukowski transformation where z and σ are the coordinates in the complex computational and physical planes, respectively. Using Jameson's method,

$$h(r,\theta)=\left|\frac{d\sigma}{dz}\right| \tag{6}$$

where $|d\sigma/dz|$ is generated numerically using a power series for general bodies.

Using this transformation and spherical coordinates, the equation for steady potential conical flow in conservative form is then

$$r\frac{\partial}{\partial r}\left[\rho r\left(\frac{\partial\phi}{\partial r}+\bar{V}_{r_\infty}\right)\right]+\frac{\partial}{\partial\theta}\left[\rho\left(\frac{\partial\phi}{\partial\theta}+\bar{V}_{\theta_\infty}\right)\right]$$
$$+2r^2H^2\rho[\phi+\bar{V}_{\bar{R}_\infty}]=0 \tag{7}$$

where $\bar{V}_{r_\infty}$, $\bar{V}_{\theta_\infty}$, and $\bar{V}_{\bar{R}_\infty}$ are the modified freestream velocity components in the $(\bar{R},r,\theta)$ system and r is defined

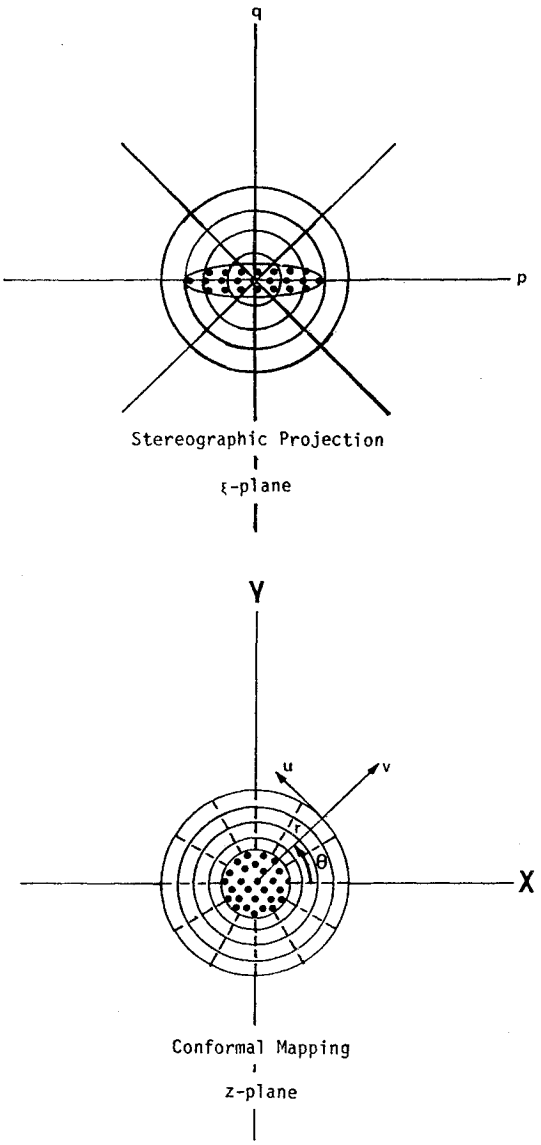

Fig. 2 Mapped planes.

in Fig. 2. The freestream velocity components as given by Grossman[1] are modified by cancellation of the metric H. In this formulation, $\bar{V}_{i_\infty}$ is therefore HV_{i_∞} where i is any one of the coordinates $\bar{R}$, r, or θ. The transformation from the $(\bar{R},\Gamma,\psi)$ system to the $(\bar{R},r,\theta)$ system is performed analytically for circles and ellipses and numerically for general bodies.

Discretization of Governing Equations

The discrete form of Eq. (7) is derived based on a conservative finite volume formulation, with the freestream discretization error explicitly subtracted. The computational grid used was set up using half-cells, as illustrated in Fig. 3. The velocity potential ϕ is defined at grid points, as are the residuals (R^n_{ij}). The density, velocity components, and metrics are all defined at cell centers.

The isentropic density ρ is modified in supersonic regions, where artificial viscosity is required for dissipation, through the artificial density

$$\tilde{\rho}=\rho-\rho_s\Delta s \tag{8}$$

Here $\rho_s\Delta s$ is the fully rotated density shift on a spherical surface and is approximated by

$$\rho_s\Delta s\approx(v_\theta/q)\delta_\theta\rho\Delta\theta r\mu_\theta\theta_{\text{fac}}+(v_r/q)\delta_r\rho\Delta r\mu_r r_{\text{fac}}$$

where

$$v_r = \frac{1}{H}[\overleftarrow{\delta_r}\phi + \overleftarrow{\delta_r}\bar{V}_{r_\infty}], \quad v_\theta = \frac{1}{rH}[\overrightarrow{\delta_\theta}\phi + \overleftarrow{\delta_\theta}\bar{V}_{\theta_\infty}] \tag{9}$$

as derived from the general curvilinear coordinate form given by Doria.[9] Doria's definitions of μ_θ and μ_r were also used. Here $\overleftarrow{\delta_\theta}$ and $\overrightarrow{\delta_\theta}$ are the usual difference operators. $\overleftarrow{\delta_r}$ and $\overrightarrow{\delta_r}$ are the negative of the usual difference operators since r increases radially outward and the mesh counter in the r direction increases from one at the outer boundary to its maximum value half a cell into the body. Here q is the magnitude of the cross-flow velocity and θ_{fac} and r_{fac} are used to tune the viscosity.

Iterative Procedure

The solution procedure for the above-defined nonlinear system follows from casting the problem in "delta" form:

$$L\Delta\phi_{ij}^{n+1} = -AR_{ij}^{n} - M \tag{10}$$

The forms of L, M, and A for the various update schemes tested are given below:

Successive line overrelaxation (SLOR)

$$L\Delta\phi_{ij}^{n+1} = \{\overleftarrow{\delta_\theta}\tilde{\rho}\overrightarrow{\delta_\theta}\}\Delta\phi_{ij}^{n+1} + \frac{r_{\text{avg}}}{\Delta r}\left\{\tilde{\rho}_{ij-\frac{1}{2}}r_{j-\frac{1}{2}}\frac{\Delta\phi_{ij-1}^{n+1} - \Delta\phi_{ij}^{n+1}/\omega}{\Delta r} - \tilde{\rho}_{ij+\frac{1}{2}}r_{j+\frac{1}{2}}\frac{\Delta\phi_{ij}^{n+1}/\omega}{\Delta r}\right\}$$

$$A = 1, \qquad M = 0 \tag{11}$$

Approximate factorization 1 (AF1)

$$L\Delta\phi_{ij}^{n+1} = (\alpha - r_{\text{avg}}\overleftarrow{\delta_r}r\tilde{\rho}\overrightarrow{\delta_r})(\alpha - \overleftarrow{\delta_\theta}\tilde{\rho}\overrightarrow{\delta_\theta})\Delta\phi_{ij}^{n+1}$$

$$A = -\alpha\omega, \qquad M = 0 \tag{12}$$

Approximate factorization 2 (AF2)

$$L\Delta\phi_{ij} = (\alpha + r_{\text{avg}}\overrightarrow{\delta_r})(-\alpha r\tilde{\rho}\overleftarrow{\delta_r} - \overleftarrow{\delta_\theta}\tilde{\rho}\overrightarrow{\delta_\theta})\Delta\phi_{ij}^{n+1}$$

$$A = -\alpha\omega, \qquad M = 0 \tag{13}$$

Checkerboard successive overrelaxation (CLSOR)

$$L\Delta\phi_{ij}^{n+1} = -\frac{1}{\omega}\left[\frac{1}{\Delta\theta^2}\{\tilde{\rho}_{i+\frac{1}{2}j} + \tilde{\rho}_{i-\frac{1}{2}j}\} + \frac{r_{\text{avg}}}{\Delta r^2}\{\tilde{\rho}_{ij-\frac{1}{2}}r_{j-\frac{1}{2}} + \tilde{\rho}_{ij+\frac{1}{2}}r_{j+\frac{1}{2}}\}\right]\Delta\phi_{ij}^{n+1}$$

$$A = 1$$

$$M = 0; \quad (i+j) = \text{odd}$$

$$M = \frac{1}{\Delta\theta^2}\{\tilde{\rho}_{i+\frac{1}{2}j}\Delta\phi_{i+1j}^{n+1} + \tilde{\rho}_{i-\frac{1}{2}j}\Delta\phi_{i-1j}^{\psi+1}\} + \frac{r_{\text{avg}}}{\Delta r^2}\{\tilde{\rho}_{ij-\frac{1}{2}}r_{j-\frac{1}{2}}\Delta\phi_{ij-1}^{n+1} + \tilde{\rho}_{ij+\frac{1}{2}}r_{j+\frac{1}{2}}\Delta\phi_{ij+1}^{n+1}\}; \quad (i+j) = \text{even} \tag{14}$$

For CKSOR, the odd points are first updated, followed by an update of the even points. α is the inverse of the pseudo-time-step for the AF schemes and ω is the overrelaxation parameter. For SLOR and AF2, the equations are implicit in the θ direction. The SLOR solution and the second stage of the AF2 solution are updated in implicit rings beginning at the outer boundary and marching into the body, coinciding with the radial flow direction. AF1 is implicit in both rings and radial lines.

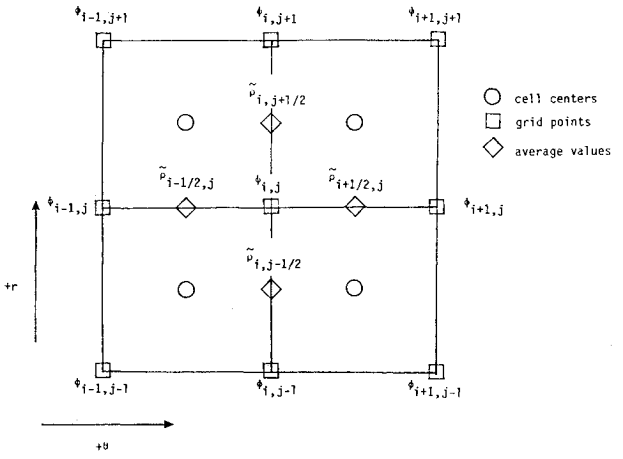

Fig. 3 Grid cell definition.

Temporal Damping

As in many transonic applications, temporal damping was required. When the potential equation is cast in "delta" form, the modified equation becomes time-like, with two pseudo-time levels in the solution.

$$\phi^{n+1} = \phi^n + \Delta\phi \tag{15}$$

The modified equation then has time derivatives that go to zero for the steady-state solution. This introduces a "time" dimension into the problem, requiring some modification in supersonic regions to establish the proper signal propagation for hyperbolic equations. For the simpler cases with no supersonic cross flow, it was generally noted that additional temporal damping in the form of ϕ_{rt} (for damping at the bow shock) was not required for schemes with natural ϕ_{rt} (SLOR and AF2), but was required and added explicitly for schemes with no natural ϕ_{rt} (CKSOR and AF1). For the flows with supersonic cross flow, $\phi_{\theta t}$ was required and added explicitly to all schemes since none of the schemes had natural $\phi_{\theta t}$.

For SLOR, ϕ_{rt} appears naturally in the update equation. These natural terms are proportional to $1/\Delta r^2$, thus the form of the explicit ϕ_{rt} coefficient is

$$\frac{\beta_r\mu}{\Delta r^2}\frac{v_r^2}{q^2} \tag{16}$$

Here β_r is the variable coefficient with the weighting of the term based on the magnitude of v_r. The same form of the coefficient was used for $\phi_{\theta t}$. The same forms used in SLOR were used for CKSOR.

The use of explicit ϕ_{rt} and $\phi_{\theta t}$ in the AF schemes required a slightly different formulation. In order to assure that temporal damping terms are the same order as the other terms (except for $\alpha^2\Delta\phi$), ϕ_{rt} and $\phi_{\theta t}$ have the forms

$$\frac{\beta_r\mu}{\Delta r}\frac{v_r^2}{q^2}; \qquad \frac{\beta_\theta\mu}{\Delta\theta}\frac{v_\theta^2}{q^2}$$

Here β_θ is defined analogously to β_r. For AF2, both ϕ_{rt} and $\phi_{\theta t}$ should be multiplied by α, the inverse pseudo-time step, to assure the same order of magnitude as the other temporal terms.

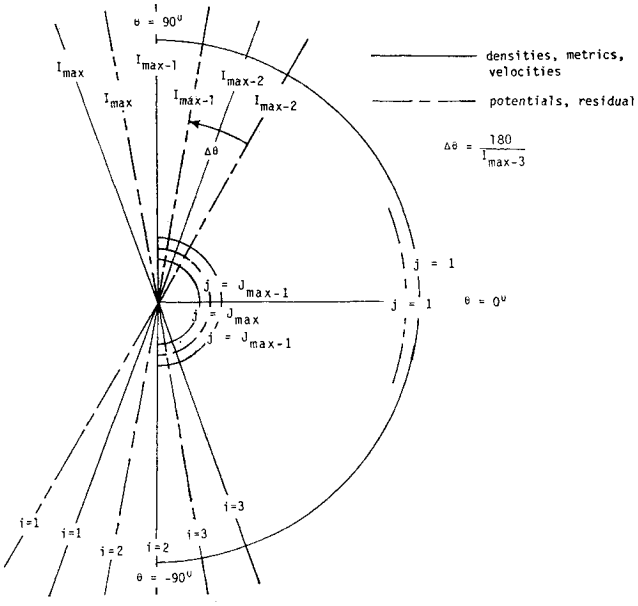

Fig. 4 Grid identification.

Boundary Conditions

For all cases studied, flow symmetry was assumed from the left half of the computational plane to the right. As shown in Fig. 4, by setting ϕ at I = 1 and 2 to ϕ at I = 3 and 4 respectively, symmetry was assured. The appropriate body surface boundary condition is:

$$\bar{V}\cdot\hat{n}=0 \tag{17}$$

For nonorthogonal curvilinear coordinates, the surface boundary condition was formulated as in Grossman's paper. The first sweep of the AF1 scheme solves for an intermediate variable, $\Delta\phi^*$, in the radial (j) direction. The intermediate condition at the surface used was $\partial\Delta\phi^*/\partial n=0$.

The first sweep of AF2 produces a bidiagonal coefficient matrix requiring an intermediate radial velocity boundary condition at the body which was $\partial\Delta\phi^*/\partial n=0$. The form of this sweep, with $\Delta\phi^*$ the intermediate variable, is

$$(\alpha+b\vec{\delta}_r)\Delta\phi^*=\alpha\omega R \tag{18}$$

For the half-cell formulation, the stability restriction, as determined by South and Hafez,[7] is

$$\alpha>b\omega/2 \tag{19}$$

For this specific problem, b is $r_{avg}/\Delta r$ since South's notation uses $\vec{\delta}_r$ as an undivided difference. An investigation of this restriction is shown in Table 1, where it is seen that the stability boundary predicted by South and Hafez is sharply defined; i.e., for cases where α violates the restriction, the solution diverges.

Results and Discussion

All four schemes were used to calculate the flow around a circle with 10 deg cone angle (CA) and 10:1 ellipses with 20 and 30 deg cone angles. The circle test cases included runs at 0 and 5 deg angle of attack (AOA) at $M_\infty=2$ and 0 and 15 deg angle of attack at $M_\infty=3$. The AOA = 15 deg case has supersonic cross flow and proved to be one of the more difficult cases to obtain a converged solution. The ellipse test cases were run at $M_\infty=2$ for AOA = 0, 5, and 10 deg on the CA = 20 deg cone and AOA = 0 and 15 deg on the CA = 30 deg cone. The CA = 20 deg cone has supersonic cross flow for the AOA = 5 and 10 deg cases and the CA = 30 deg cone for the AOA = 15 deg. The AOA = 15 deg ellipse case was the most difficult of the ellipse solutions obtained. Several different grids were tested to determine the effects of grid spacing on convergence and accuracy. The 63×31 grid was chosen as the basic grid for all solutions since the solutions were generally obtained quickly and yet reliably. The domain was taken to be a half-plane extending from $\phi=(-90$ deg $+\Delta\theta)$ to $\theta=(90$ deg $+\Delta\theta)$ over 63 grid points and from the body to some outer radial distance defined by tan $\psi/2$ over 31 grid points. For circles at 0 deg angle of attack, the flow is totally radial and 13×31 grids were used since each radial ray has the same solution.

Scalar and vector times for the various parts of the calculation are listed in Table 2. The times are normalized with respect to the scalar residual time. The increase in speed through vectorization is notable. Since these two dimensional solutions generally require little CPU time on the CYBER-203, the increase in speed through vectorization can best be observed by comparing the speed of the various segments of the code rather than the entire CPU time. The segments of the code which are completely vectorizable—freestream velocity and metrics, artificial density, and residual—are a factor of two to three faster in vector form. The freestream velocity speed-up is a factor of ten because the forms of the Fortran-supplied functions used (sine, cosine) are much faster in vector form. The three implicit update schemes—SLOR, AF1, and AF2—are slightly faster vectorized (where possible), as expected. The CKSOR update scheme, which is completely vectorizable, is about three times faster than its scalar form. These increases in speed through vectorization are about what is expected for the CYBER-203, which has a nominal vector to scalar speed ratio of about three.

General observations for the required optimized parameters for each scheme are discussed here. Modifications to the artificial density using θ_{fac} and r_{fac} are required for AF1, AF2, and CKSOR for both subsonic and supersonic cross flow. For subsonic cross flow, $\theta_{fac}=r_{fac}=2$. For supersonic cross flow, $\theta_{fac}=4$ and $r_{fac}=2$. For SLOR, $\theta_{fac}=4$ for supersonic cross flow cases and $r_{fac}=1$ for all cases. The overrelaxation parameter for AF1 and AF2 was found to be optimal at $\omega=1.7$ for all cases. For SLOR and CKSOR, the overrelaxation parameter was found to be optimal around $\omega=1.95$ for the entire grid. This parameter was lowered to around $\omega=1.75$ for some of the more difficult cases for SLOR and CKSOR. The switch Mach number for the artificial density varied in the range $0.9\le sw\le1$. Switch Mach numbers less than one were generally used for flows with supersonic cross flow. $\phi_{\theta t}$ was required only for supersonic cross flow. Explicit ϕ_{rt} was required for all flows in AF1 and CKSOR since it does not occur naturally. Additional ϕ_{rt} was required for AF2 and SLOR for flows with strong bow shocks. The optimal α range for the AF schemes was determined to be between $\alpha_{min}=5$ for both AF1 and AF2 and $\alpha_{max}=1/\Delta r^2$ for AF1, and $\alpha_{max}=1/\Delta r$ for AF2. For the 30 deg CA ellipse cases, $\alpha_{min}=20$ and $\alpha_{max}=6.25/\Delta r^2$ for AF1; for the 30 deg CA ellipse, 15 deg AOA, $M_\infty=2$, $\alpha_{min}=15$, and $\alpha_{max}=2.5/\Delta r$ for AF2. These were the only variations in α_{min} and α_{max}. A geometric sequence of eight parameters was used to determine the α sequence:

$$\alpha=\alpha_{max}[\alpha_{min}/\alpha_{max}]^f \tag{20}$$

where

$$f=\frac{\text{iteration}-(\text{iteration/no. parameters})\times\text{no. parameters}}{\text{no. parameters}-1} \tag{21}$$

Three parameters were used for the circle at 0 deg AOA for AF1 and for the 0 deg AOA, $M_\infty=3$ circle case for AF2. The outer boundary of the grid varied depending on the Mach number, the angle of attack, and the cone angle of the

Table 1 Test of AF2 intermediate body boundary condition stability criterion ($M_\infty = 2.0$, AOA = 0 deg circle)

					$\alpha > b\omega/2$		$\alpha < b\omega/2$	
IMAX	JMAX	b	ω	$b5\omega/2$	α	Result	α	Result
13	51	18.8	1.0	9.4	10.35	C	8.5	D
↓	↓	↓	1.7	16	17.6	C	14.4	D
			1.95	18.33	20.16	C	16.5	D

Table 2 Scalar vs vector CPU times (63 × 31 grid)

Operation	CYBER-203 normalized scalar time, s	CYBER-203 normalized vector time, s
Calculation of freestream velocity and metrics	33.26	2.551
Calculation of (per iteration):		
Artificial density	4.493	1.449
Residual	1.000	0.594
SLOR update	4.638	4.174
CKSOR update	4.014	1.261
AF1 update	4.710	2.957
AF2 update	6.000	3.652

body. Care was taken to ensure that the outer boundary was outside the entire bow shock. An erroneous solution was obvious by examination of a Mach chart should the bow shock not be entirely within the grid. The affect of outer boundary shape on convergence rate was not investigated in this study. The outer boundary was determined for the circles by tan $r_{max}/2$.

In order to obtain solutions with optimal convergence rates, SLOR and CKSOR required adjustment of eight parameters; AF1 and AF2 eleven parameters. Most of the parameters could be used from case to case without changing, but β_r and β_θ had to be optimized for each case. SLOR seemed to be the least sensitive to these parameters, and remained stable for almost any value of β_r and β_θ. CKSOR, AF1, and AF2 were extremely sensitive to β_r and β_θ. CKSOR becomes unstable outside a small range for both parameters while AF1 and AF2 become unstable outside a small range for β_θ. The sensitivity of AF1 and AF2 to β_r is illustrated in Fig. 5 for the $M_\infty = 2$, AOA = 15 deg, CA = 30 deg ellipse case. For relatively small changes in β_r, the number of iterations required for solution increased significantly. Optimization of β_r and β_θ was a rather lengthy procedure for the AF schemes. The terms proportional to β_r and β_θ are required for stability, but tend to slow convergence. Thus, optimal convergence rate is obtained when β_r and β_θ are the minimal values required for stability. For reliability and robustness viewpoints and for ease of determining parameters to get a converged solution, SLOR should be the choice over AF1, AF2, and CKSOR.

Circles

The performance of the various schemes for circles in terms of residual histories is shown in Fig. 6-8. The criterion for a converged solution is a maximum absolute residual no greater than 10^{-4} anywhere on the grid. This has been found to give aerodynamic convergence; i.e., the bow shock and any cross-flow shocks are properly located and the pressure distribution is converged to four decimal places. The schemes have been tested, however, by further reducing the residual in order to establish the stability of the scheme and as a further test of a converged solution. The AF2 scheme converges in the fewest number of iterations for the $M_\infty = 2$, AOA = 0 and 5 deg cases. AF2 is followed by AF1, SLOR, and CKSOR. For the $M_\infty = 3$, AOA = 0 deg case, AF1 produced the converged solution in the fewest iterations, followed by AF2, SLOR, and CKSOR. This was the only solu-

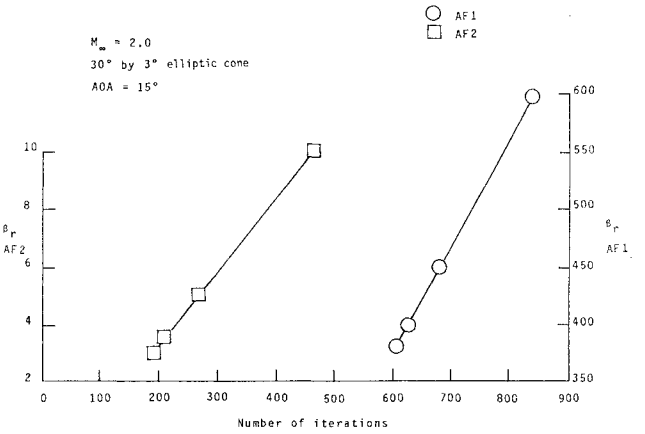

FIg. 5 Sensitivity of AF schemes to ϕ_{rr}.

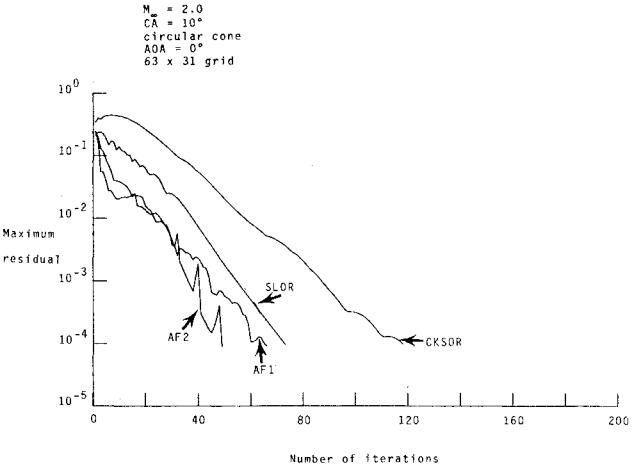

Fig. 6 Maximum residual vs number of iterations, 10 deg circular cone, Mach 2, 0 deg AOA.

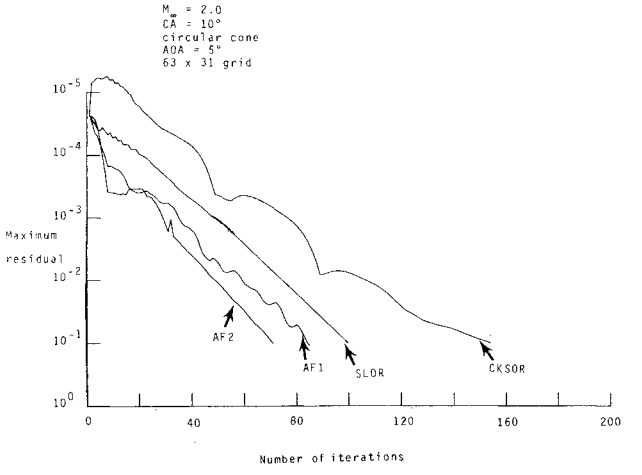

Fig. 7 Maximum residual vs number of iterations, 10 deg circular cone, Mach 2, 5 deg AOA.

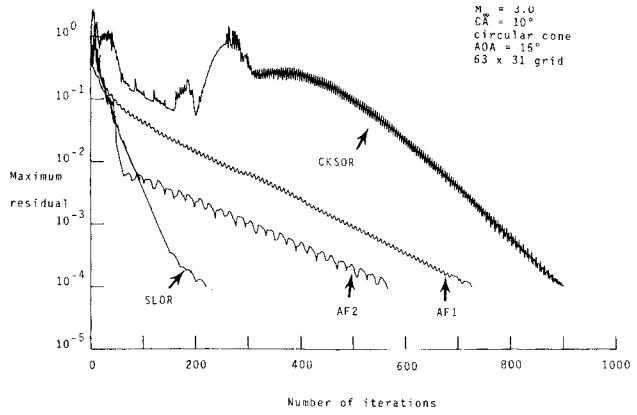

Fig. 8 Maximum residual vs number of iterations, 10 deg circular cone, Mach 3, 15 deg AOA.

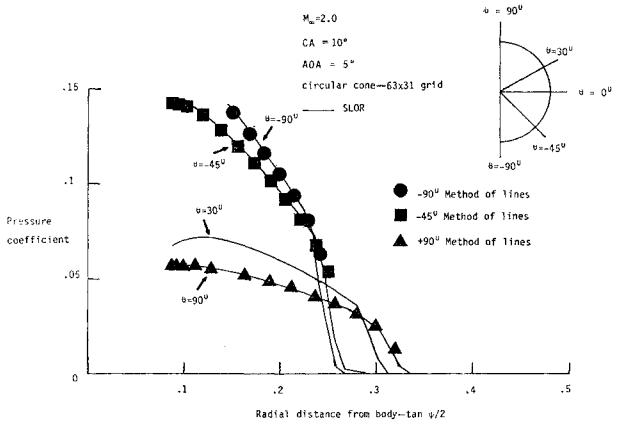

Fig. 9 Pressure coefficient vs radial distance from body, 10 deg circular cone, Mach 2, 5 deg AOA, $\theta = -90, -45, 30, 90$ deg.

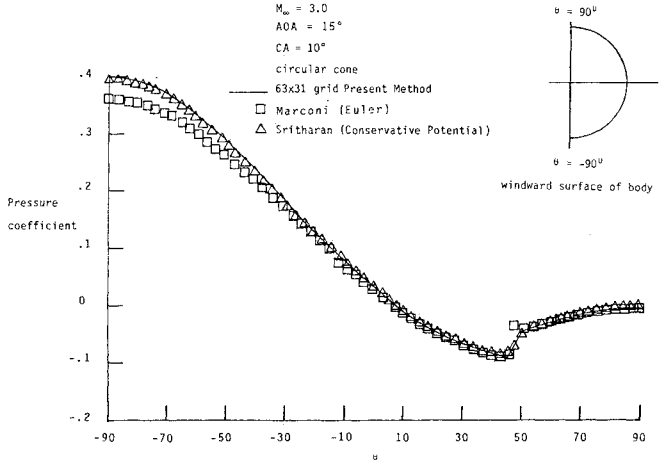

Fig. 10 Pressure coefficient vs circumferential angle, 10 deg circular cone, Mach 3, 15 deg AOA.

tion of all the test cases in which the AF1 scheme converged in the fewest number of iterations.

The $M_\infty = 3$ bow shock is much stronger than the $M_\infty = 2$ bow shock, and it is suspected that the natural θ_{rt} of AF2 is very close to the miminum amount required for stability, yielding the AF1 scheme slightly better with its explicitly added ϕ_{rt}. For the AOA = 15 deg case at $M_\infty = 3$, the supersonic cross flow and stronger bow shock require the addition of explicit ϕ_{rt} and $\phi_{\theta t}$ for stability. The residual history for the four schemes is shown in Fig. 8. The effect of adding large quantities of ϕ_{rt} and $\phi_{\theta t}$ to the AF schemes is apparent as the two schemes are slower by a factor of two for AF2

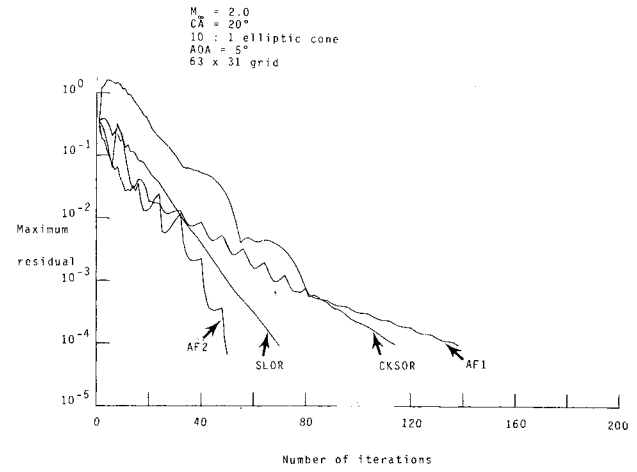

Fig. 11 Maximum residual vs number of iterations, 20 deg elliptic cone, Mach 2, 5 deg AOA.

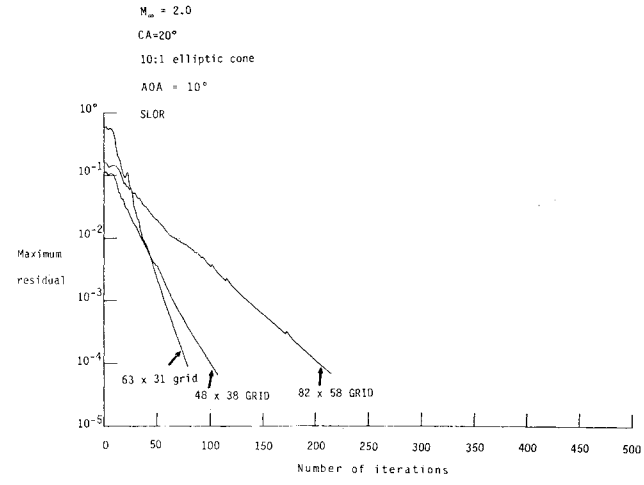

Fig. 12 Maximum residual vs number of iterations, 20 deg elliptic cone, Mach 2, 10 deg AOA, SLOR, different grids.

and three for AF1 when compared to SLOR. The circle proves to be a very difficult conical case since the radius of curvature of the body is constant, leading to a residual dominated by low frequency error. As will be shown for the ellipses, the change in radius of curvature of the thinner body allows the solution to proceed more quickly. The determination of the optimum ϕ_{rt} and $\phi_{\theta t}$ required many more runs of AF1 and AF2 than the optimum for SLOR, demonstrating the superior reliability and robustness of SLOR. The CKSOR scheme required four times the number of iterations, indicating that even vectorization would not make it faster in CPU time than SLOR.

Pressure coefficients plotted against the radial distance from the body surface are shown in Fig. 9 for the $M_\infty = 2$, AOA = 5 deg case. Data from Jones[10] are plotted for the $\theta = -90, -45, +90$ deg rays for comparison with the present method. Agreement is quite good.

The surface pressure coefficient plotted against the angle around the circle from $\theta = -90$ to $+90$ deg is shown for the $M_\infty = 3$, AOA = 15 deg case in Fig. 10. Data are presented using the present method, a shock-fit Euler solution provided by Marconi, and a conservative potential solution provided by Sritharan. The solution agrees well with that provided by Sritharan and differs from the Euler solution only on the lower surface where the bow shock is strongest. Smearing of the cross-flow shock is evident in both potential solutions, which otherwise predict the proper pressure levels.

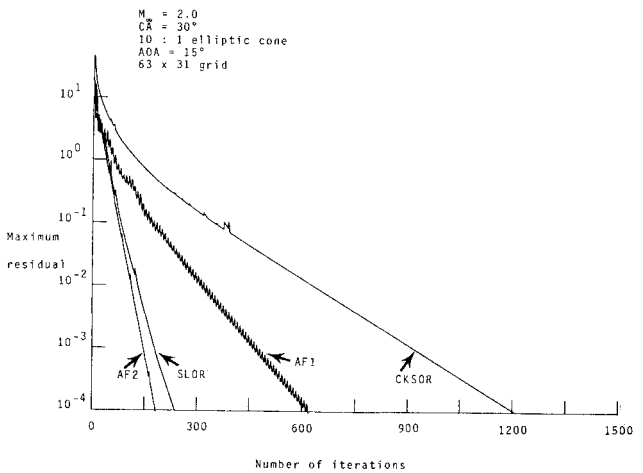

Fig. 13 Maximum residual vs number of iterations, 30 deg elliptic cone, Mach 2, 15 deg AOA.

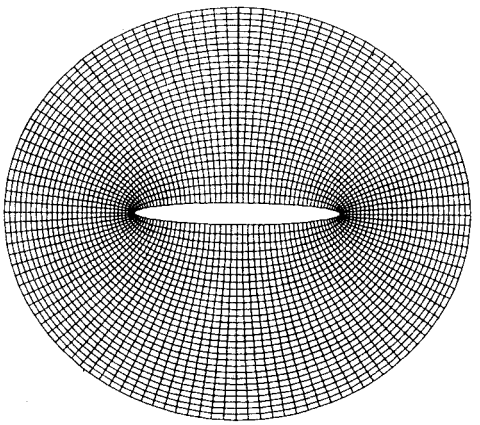

Fig. 14 Coordinate system for elliptic cone, 63×31 grid.

Ellipses

Residual histories for the four schemes for the various ellipses at various angles of attack and $M_\infty = 2$ are shown in Figs. 11-13. For all ellipse test cases, AF2 converges in the fewest iterations, with SLOR only slightly slower. AF1 and CKSOR require many more iterations for almost every case. The 63×31 grid for the ellipse cases is shown in Fig. 14. For the AOA = 10 deg case, as shown in Fig. 12, various grids were tested using SLOR to see the variation in number of iterations with different grids. The 63×31 grid is compared to 48×38 and 82×58 grids, with the 63×31 grid requiring the fewest number of iterations. The solutions differ only slightly, with more grid points in the θ direction giving a sharper cross-flow shock, as expected, but pressure levels and shock locations the same as the 63×31 grid. The variation in number of iterations with angle of attack for the CA = 20 deg ellipse for all four schemes is illustrated in Fig. 15. Both the AOA = 5 and 10 deg cases have supersonic cross-flow. The robustness of both SLOR and AF2 is easily seen, as the more complicated supersonic cross-flow cases require only slightly more iterations for convergence. The AF1 and CKSOR schemes are significantly affected by the presence of supersonic cross-flow and require many more iterations for convergence. CKSOR vectorized would still be generally slower than SLOR and AF2.

The surface pressure coefficients vs X/XLE ($X/X_{\text{leading edge}}$), where X is the real part of z in the stereographed plane, for the CA = 20 deg ellipse, $M_\infty = 2$, AOA = 5 and 10 deg is shown in Fig. 16, along with the nonconservative potential

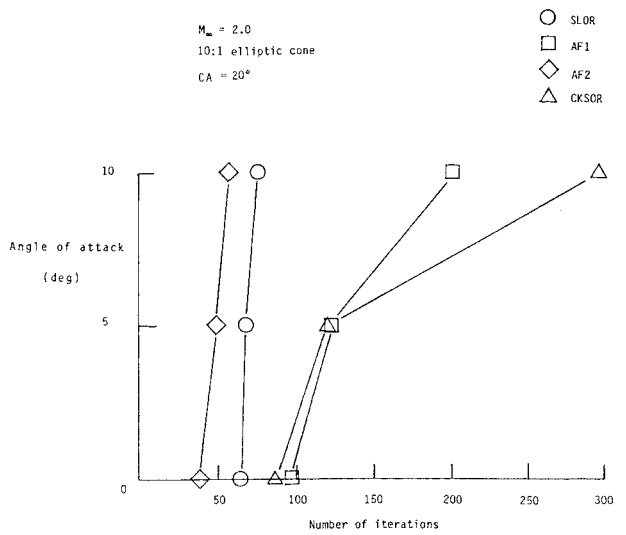

Fig. 15 Variation in number of iterations with angle of attack, Mach 2, 20 deg elliptic cone.

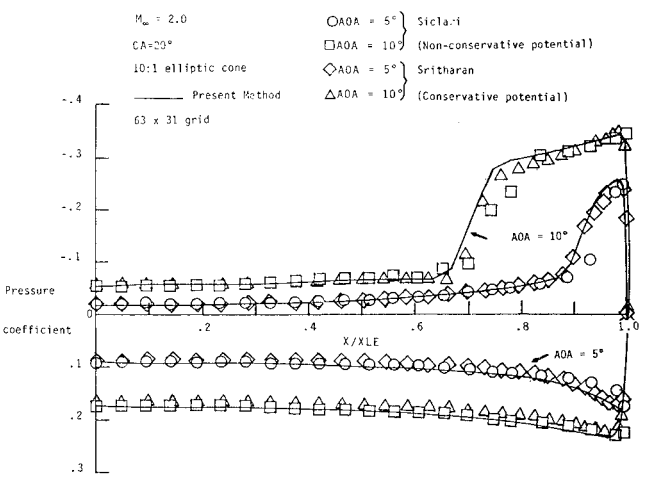

Fig. 16 Pressure coefficient vs X/XLE, 20 deg elliptic cone, Mach 2, 5, 10 deg AOA.

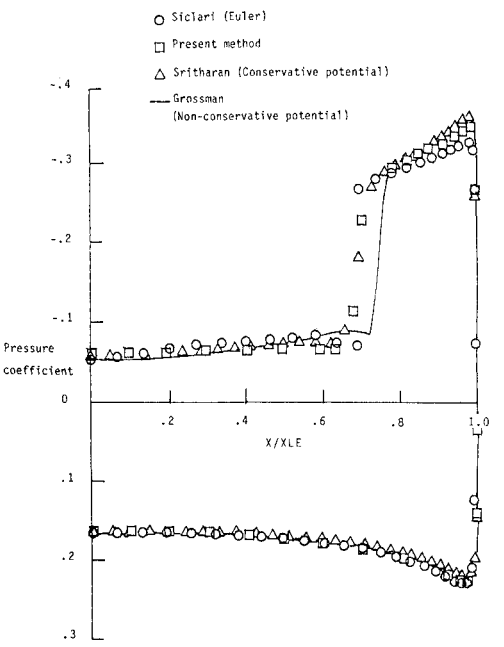

Fig. 17 Pressure coefficient vs X/XLE, 20 deg, 1.5 deg elliptic cone, Mach 2, 10 deg AOA.

solution of Siclari and the conservative potential solution of Sritharan. The present method agrees well with both solutions. The location of the cross-flow shock is slightly inboard of the nonconservative solution, as expected. The present method is also slightly different from that of Sritharan. Sritharan does not use stereographic projection to an intermediate plane. This will cause a slight difference in ellipse sizing, since the stereographed 10:1 ellipse is 20×2.0845 deg rather than 20×2 deg as used by Sritharan. In Fig. 17, the solution for 20×1.5 deg ellipse at $M_\infty = 2$, AOA = 10 deg is shown. The plot includes data from the present method, the conservative potential of Sritharan, the nonconservative potential of Grossman, and the Euler solution of Siclari. Agreement with the code of Sritharan is much better for this ellipse since the ellipse dimensions between codes are identical. Both conservative potential solutions give good agreement with the Euler shock location and are slightly inboard of the nonconservative potential shock location.

Conclusions

A method has been developed to solve the steady conservative potential equation for supersonic conical flow using the artificial density method. The code has been vectorized for processing on CYBER-200 series computers. Four update schemes previously used mainly for transonic flow calculations have been tested for speed, robustness, and vectorizing capability. The SLOR scheme is most easily implemented. It is the most reliable and robust and even though it is only partially vectorizable, due to its inherently higher convergence rate, it is faster than CKSOR, which is totally vectorizable. The AF2 scheme tested is much more reliable and robust than the AF1 scheme tested. The AF2 scheme is generally the fastest of all the schemes tested, but is sensitive to parameter definitions. For future work in three-dimensional conservative full-potential codes which require vectorization for speed, SLOR appears the best choice for the basic update scheme. The AF2 scheme would be a good optional scheme for the production code due to its speed. Sensitivity to its parameters, however, makes AF2 generally more difficult to run than SLOR.

The codes developed in this study have been shown to have good agreement with other potential codes of both the conservative and nonconservative types and Euler codes.

References

[1]Grossman, B., "Numerical Procedure for the Computation of Irrotational Conical Flows," *AIAA Journal*, Vol. 17, Aug. 1979, pp. 828-837.

[2]Siclari, M. J., "Approximate-Factorization Schemes for 3-D Nonlinear Supersonic Potential Flow," AIAA Paper 83-0376, Jan. 1983.

[3]Sritharan, S. S. and Seebass, A. R., "A Finite Area Method for Nonlinear Conical FLows," AIAA Paper 82-0995, June 1982.

[4]Jameson, A., "Iterative Solution of Transonic Flows Over Airfoils and Wings Including Flows at Mach 1," *Communications of Pure and Applied Mathematics*, Vol. 27, 1974, pp. 283-309.

[5]Shankar, V., "Conservative Full-Potential, Implicit Marching Scheme for Supersonic Flows," *AIAA Journal*, Vol. 20, Nov. 1982, pp. 1508-1514.

[6]Hafez, M. M., Murman, E. M., and South, J. C., "Artificial Compressibility Methods for Numerical Solution of Transonic Full-Potential Equation," *AIAA Journal*, Vol. 17, Aug. 1979, pp. 838-906.

[7]South, J. C. and Hafez, M. M., "Stability Analysis of Intermediate Boundary Conditions in Approximate Factorization Schemes," AIAA Paper 83-1898-CP, July 1983.

[8]Weatherburn, C. E., *Differential Geometry of Three Dimensions*, Vol. 1, University Press, Cambridge, England, 1955, pp. 167-173.

[9]Doria, M. L. and South, J. C., "Transonic Potential Flow and Coordinate Generation for Bodies in a Wind Tunnel," AIAA Paper 82-0223, Jan. 1982.

[10]Jones, D. J., "Tables of Inviscid Supersonic Flow About Circular Cones at Incidence $\gamma = 1.4$," NATO AGARDOgraph 137, 1969.